



PCCP

**Thermodynamics, dynamics, and structure of supercritical water at extreme conditions**

Journal:	<i>Physical Chemistry Chemical Physics</i>
Manuscript ID	CP-ART-04-2020-002288.R1
Article Type:	Paper
Date Submitted by the Author:	15-Jun-2020
Complete List of Authors:	Yoon, Tae Jun; Los Alamos National Laboratory, Material Physics and Applications Division Patel, Lara; Los Alamos National Laboratory Ju, Taeho; Los Alamos National Laboratory, Material Physics and Applications Division Vigil, Matthew; Los Alamos National Laboratory, Material Physics and Applications Division Findikoglu, Alp; Los Alamos National Laboratory, Material Physics and Applications Division Maerzke, Katie; Los Alamos National Laboratory Currier, Robert; Los Alamos National Laboratory

SCHOLARONE™  
Manuscripts

Cite this: DOI: 00.0000/xxxxxxxxxx

# Thermodynamics, dynamics, and structure of supercritical water at extreme conditions<sup>†</sup>

Tae Jun Yoon,\* Lara A. Patel, Taeho Ju, Matthew J. Vigil, Alp T. Findikoglu, Robert P. Currier, and Katie A. Maerzke

Received Date

Accepted Date

DOI: 00.0000/xxxxxxxxxx

Molecular dynamics (MD) simulations to understand the thermodynamic, dynamic, and structural changes in supercritical water across the Frenkel line and the melting line have been performed. The two-phase thermodynamic model [*J. Phys. Chem. B* (2010), **114**(24), 8191-8198] and the velocity autocorrelation functions are used to locate the Frenkel line and to calculate the thermodynamic and dynamic properties. The Frenkel lines obtained from the two-phase thermodynamic model and the velocity autocorrelation criterion do not agree with each other. Structural characteristics and the translational diffusion dynamics of water suggest that this inconsistency could arise from the two oscillatory modes in water, which are associated with the bending of hydrogen bonds and intermolecular collisions inside the first coordination shell. The overall results lead us to conclude that the universality of the Frenkel line as a dynamic crossover line from rigid to nonrigid fluids is preserved in water.

## 1 Introduction

Supercritical water, a fluid state above the gas-liquid critical point, is of great importance for its industrial uses<sup>1,2</sup> and its occurrence in nature.<sup>3,4</sup> Seawater in the vicinity of a hydrothermal vent is supercritical and water in the Earth's crust and mantle is either a supercritical fluid or a high-pressure ice.<sup>5,6</sup> Thus, supercritical water has a tremendous effect on geological processes and deep-sea ecosystems.<sup>5</sup> From an industrial point of view, the anomalous properties of near-critical and supercritical water have been exploited for chemical synthesis,<sup>2</sup> desalination,<sup>7</sup> and pollutant oxidation.<sup>8</sup> The peculiarity of supercritical water has been extensively studied in the field of chemical physics and physical chemistry. For instance, the hydrogen bonding network and its role in supercritical water continue to be debated.<sup>9,10</sup> Recently, a series of studies have been devoted to identifying the supercritical gas-liquid transition line (region), also known as the Widom line ( $\delta$ ).<sup>11-19</sup> On the other hand, the characteristics of dense supercritical water have not been as well studied.

This work aims to understand the behavior of supercritical wa-

ter in a variety of conditions, from gas-like to solid-like. Specifically, we are interested in two crossover lines including the Frenkel line (FL), a rigid-nonrigid dynamic crossover line,<sup>20,21</sup> and the melting line. The FL concerns the dynamic duality of liquids. The liquid state has been understood from two opposite points of view. Van der Waals regarded the liquid as a compressed gas,<sup>22</sup> whereas Frenkel deemed it close to a solid. Frenkel argued that the dynamics of a liquid resembles that of a defect-ridden solid when its structural relaxation time ( $\tau$ ) is comparable to the shortest vibration period ( $\tau_0$ ) in the solid.<sup>23</sup> Based on Frenkel's idea, Brazhkin et al. first located the FL by defining it as a set of thermodynamic states where  $\tau$  becomes comparable to  $\tau_0$ .<sup>24</sup> In subsequent studies, they suggested thermodynamic and dynamic criteria to locate the FL,<sup>24,25</sup> but these criteria were criticized by Bryk et al.<sup>26-28</sup> A series of recent works<sup>29-34</sup> also proposed several thermodynamic, geometric and dynamic changes associated with the FL. It is noteworthy that several recent works aim to understand the dynamic crossover in conjunction with thermodynamic scaling theory or the isomorph theory.<sup>35-38</sup> Brazhkin et al.<sup>33</sup> note that the thermodynamic states where several transport properties of soft-sphere particles (the logarithm of self-diffusion coefficient, shear viscosity, and kinematic viscosity) show qualitative changes are related to the Frenkel line they defined. Bell et al.<sup>34</sup> do not use the term *Frenkel line* but suggests a dynamic crossover line based on a similar idea to Brazhkin et al.<sup>33</sup> They use the excess entropy scaling for the determination of a dynamic crossover line. Our recent work<sup>39</sup> directly shows that the Frenkel lines of simple soft-sphere fluids and their melting lines are iso-

Los Alamos National Laboratory, P.O. Box 1663 Los Alamos, NM 87545, the United States

\*E-mail: tyoon@lanl.gov

<sup>†</sup> Electronic Supplementary Information (ESI) available: (1) the number of hydrogen bonds (HBs) per molecule from a single distance criterion ( $r_{O...H} < 2.2 \text{ \AA}$ ); (2) the timestep validation results; (3) the influence of the bond flexibility on the dynamic behavior of supercritical water; and (4) numerical data obtained from the two-phase thermodynamic (2PT) model and structural parameters of the TIP4P/2005 water model. See DOI:

morphic. Since the FL is related to a qualitative change in the behavior of dense fluids in extreme environments and the scaling theory of dynamic properties, therefore, it is important to understand the dynamic crossover and locate the FL. Despite the importance and the soundness of the notion, there remain several challenging issues related to the FL.<sup>26</sup>

Many proposed criteria yield FLs that are not in agreement. First, the  $\tau = \tau_0$  definition, the cornerstone of Frenkel's idea,<sup>26</sup> cannot be determined in a quantitatively rigorous way from the mean square displacement and often lies far from FLs determined by other criteria. Poor agreement was reported with both the heat capacity criterion ( $C_v = 2.0 k_B$  for monatomic fluids) and the velocity autocorrelation function [ $Z(t)$ ] criterion, which are most frequently used to define the FL (see Sec. 2.3 for a description of the  $Z(t)$  criterion). Brazhkin et al.<sup>40</sup> attributed the discrepancy to calculation error ( $\approx 10\%$ ), but this does not fully account for the discrepancy.<sup>41</sup> Our recent work<sup>32</sup> demonstrates that the two-phase thermodynamic (2PT) model for monatomic fluids<sup>42</sup> can locate the FL of simple monatomic fluids in agreement with the recent discussion related to the isomorph theory. However, the ability of the 2PT model to locate the FL was not validated for polyatomic species in which more degrees of freedom in motion exist.

The second issue relates to terminology. Brazhkin et al.<sup>24</sup> first used the term *rigid-nonrigid* crossover for the FL, but denoted it as a *gas-liquid* transition line in subsequent works.<sup>20,21,25,40</sup> Indeed, both terms are frequently used interchangeably.<sup>23</sup> This mixed use of terminology sometimes conflicts with usage in gas-liquid criticality or the Widom line.<sup>19</sup>

Another issue, which is especially relevant to water, concerns the universality of the  $Z(t)$  criterion. As described earlier, recent studies regard that the FL is closely related to thermodynamic scaling theory. The thermodynamic scaling theory states that the dynamics of a simple liquid can be represented as a unique function of  $\rho^{\gamma_{\text{scale}}}/T$  where  $\gamma_{\text{scale}}$  is called the density scaling exponent. Thus, the parallelism between the FL and the ML on the  $\rho - T$  and  $p - T$  planes suggests that the thermodynamic states at the FL have the same density scaling exponent ( $\gamma_{\text{scale}}$ ) with those at the ML in simple fluid models. On the other hand, the FL in water from the  $Z(t)$  criterion is quite dissimilar to that in simple fluids.<sup>20,21</sup> For instance, the ML is not parallel to the FL on the pressure-temperature diagram. Considering that the FL shows similar behavior in soft-sphere and hard-sphere fluids, the disagreement casts into question the validity of the  $Z(t)$  criterion.

For the melting line of high-temperature/high-pressure water, there have been a series of recent studies on the solid-liquid transition of water under extreme conditions.<sup>43-45</sup> A plastic crystal phase (PC) was proposed as a new state of ice that appears above 350 K and 60 kbar.<sup>43-45</sup> In the PC, water molecules lose their translational degrees of freedom but rotate freely.

In order to address these issues, we use the  $Z(t)$  criterion and the two-phase thermodynamic (2PT) model for polyatomic species for the thermodynamic and dynamic characterization of the FL.<sup>46</sup> The ML is characterized by examining the discontinuity in thermodynamic variables [e.g., pressure ( $p$ ), density ( $\rho$ ), internal energy ( $E$ ), enthalpy ( $H$ ), and free energy ( $G$  and  $A$ )]. We

demonstrate that the 2PT model for polyatomic species not only locates the FL but also explains its physical meaning. Simultaneously, we find that the FLs determined by these two methods do not agree with each other. Based on the structural and dynamic analyses, we show that both FLs have their own physical meanings but that the FL from the 2PT model conserves the universal characteristics that are observed in simple and non-associating fluids.

## 2 Methods

### 2.1 Molecular dynamics (MD) simulations

The Large-scale Atomic/Molecular Massively Parallel Simulator (LAMMPS, 12 Dec 2018) is used for all simulations.<sup>47</sup> The TIP4P/2005 model,<sup>48</sup> one of the most popular rigid nonpolarizable water models,<sup>12,49</sup> is mainly used to model the interatomic potential. All simulations are repeated at least three times with different initial configurations and velocity distributions. The timestep ( $\Delta t$ ) is 1 fs in the following  $NVT$  and  $NpT$  simulations. Long-range Coulomb interactions are computed using the particle-particle particle-mesh (pppm) solver with a tolerance parameter of  $10^{-5}$  in all simulations.

In the  $NVT$  simulations, both the standard 12-6 Lennard-Jones interaction and the Coulombic pairwise interaction are cut at 14 Å and the tail correction term is added. The number of water molecules is 2,000 ( $N = 2,000$ ). The simulation temperatures and densities are  $T_r = 1.0 - 5.0$  and  $\rho_r = 0.1 - 9.4$ . For all symbols,  $P_r$  denotes the reduced property ( $P_r = P/P_c$ ) where  $P_c$  is the property at the critical point. The critical point is estimated using the flat top proposal<sup>16,50</sup> ( $\rho_c = 284.23 \text{ kg/m}^3$ ,  $p_c = 178.90 \text{ bar}$ , and  $T_c = 654.10 \text{ K}$ ). In the  $NVT$  simulations, the initial configurations are first relaxed for 4 ns. Next, the simulations are run to obtain the internal energy, pressure, and trajectory data for the structural analysis. The trajectory data is collected every 10 ps for 2 ns. An additional run of the  $NVT$  simulation is performed to collect the trajectory data every single step for 30 ps to calculate thermodynamic properties including absolute entropy, Helmholtz free energy, and Gibbs free energy.

The  $NpT$  simulations are conducted to determine the melting temperature following the simulation procedure introduced by Takii et al.<sup>45</sup> Three different initial configurations of 512 molecules are prepared at each thermodynamic condition. These initial configurations are equilibrated for a few ns ( $\geq 4 \text{ ns}$ ) at the thermodynamic conditions in the vicinity of the melting line obtained from the first set of  $NVT$  simulations. The simulation pressures range from 100 kbar to 700 kbar with an interval of 100 kbar. The Nosé-Hoover thermostat and barostat are used to control the temperature and pressure. Both Coulombic and short-range interactions are cut at 8 Å and the tail correction term is added following the earlier studies on the plastic crystal formation<sup>43-45</sup>. The trajectory data and the system volume are collected during the production run (2 ns). As with the first set of simulations, the trajectory data are collected every single step for 30 ps to calculate absolute entropy. Note that the cutoff distance and the number of molecules in the  $NpT$  simulations have been reduced from the values used in the  $NVT$  simulations. They were re-

duced under the hypothesis that the solid-liquid transition at high temperature is dominated not by the long-range attractive interaction but by the short-range attractive and repulsive interactions. Aragones et al.<sup>43</sup> demonstrated that including the attractive interaction beyond the cutoff radius has little change ( $\sim 1.5\%$ ) on the coexistence densities, which is acceptable for the goal of this work. This hypothesis will be validated by comparing the melting lines obtained from the *NVT* simulations to those from the *NpT* simulations.

Simulations of a shorter timestep ( $\Delta t = 0.5$  fs) are additionally performed at  $T_r = 1.0$  to examine the effect of the timestep size. No significant effect was observed for all conditions (see the Table S1 in the ESI<sup>†</sup>) as shown in our previous work involving simple Lennard-Jones fluids.

In addition to the TIP4P/2005 model, we also perform MD simulations using the SPC/Fw model,<sup>51</sup> a flexible variant of the SPC/E model, to examine the influence of the intramolecular flexibility at  $T = 298.15$  K and over the range of  $T = 654.1 - 2616.4$  K. The influence of the flexibility on the fluidicity parameter is not significant as shown in Table S2 and Fig. S2 (see the ESI<sup>†</sup>), which agrees with the results obtained by Lin et al.<sup>46</sup> and Pascal et al.<sup>52</sup> Since the calculation of thermodynamic contributions from the intramolecular vibration is computationally intensive and the result does not contribute substantially to the thermodynamic properties, we mainly focus on using the TIP4P/2005 model throughout the main article.

It should be noted that non-reactive water models are not realistic under extreme conditions. For instance, 25 % of the water molecules decompose into hydrogen and oxygen at  $\sim 2500$  K ( $T_r \sim 3.9$ ) and 0.05 bar.<sup>53,54</sup> Still, the rigid nonpolarizable model may provide useful insight into the behavior of supercritical water under extreme conditions.

## 2.2 Two-phase thermodynamic (2PT) model

The 2PT model for polyatomic species<sup>46</sup> calculates the thermodynamic properties based on the vibrational density of states ( $\Psi$ ) of each type of motion (translation (t), rotation(r), and intramolecular vibration (v)) [Eq. (1)].

$$\Psi(\nu) = \Psi^t(\nu) + \Psi^r(\nu) + \Psi^v(\nu) \quad (1)$$

In Eq. (1),  $\nu$  is the frequency. The vibrational density of states of each type of motion is obtained by Fourier transforming either the spectral density or the velocity autocorrelation functions. The density of states of the translational, rotational, and intramolecular vibrational motions are defined as:

$$\Psi^t(\nu) = \frac{1}{k_B T} \lim_{\tau \rightarrow \infty} \sum_{j=1}^N \sum_{k=1}^3 \frac{M_j}{\tau} \left| \int_{-\tau}^{\tau} v_{t,j}^k(t) e^{-2\pi i \nu t} dt \right|^2 \quad (2a)$$

$$\Psi^r(\nu) = \frac{1}{k_B T} \lim_{\tau \rightarrow \infty} \sum_{j=1}^N \sum_{k=1}^3 \frac{I_j^k}{\tau} \left| \int_{-\tau}^{\tau} \omega_j^k(t) e^{-2\pi i \nu t} dt \right|^2 \quad (2b)$$

$$\Psi^v(\nu) = \frac{1}{k_B T} \lim_{\tau \rightarrow \infty} \sum_{\ell=1}^{3N} \sum_{k=1}^3 \frac{m_\ell}{\tau} \left| \int_{-\tau}^{\tau} v_{v,\ell}^k(t) e^{-2\pi i \nu t} dt \right|^2 \quad (2c)$$

In Eq. (2),  $T$  is the temperature,  $i$  is the imaginary unit ( $i^2 = -1$ ),  $k_B$  is the Boltzmann constant,  $M_j$  is the mass of the  $j^{\text{th}}$  molecule,  $m_\ell$  is the atomic mass of the  $\ell^{\text{th}}$  particle,  $I_j^k$  is the  $k^{\text{th}}$  principle moment of inertia of the  $j^{\text{th}}$  molecule,  $v_{t,j}^k$  and  $\omega_j^k$  are the translational velocity of the center of mass and the angular velocity of the  $j^{\text{th}}$  molecule in the  $k^{\text{th}}$  direction at time  $t$ .  $v_{v,\ell}^k(t)$  is the  $k^{\text{th}}$  directional component of the intramolecular vibrational velocity of the  $\ell^{\text{th}}$  atom at time  $t$ . The intramolecular vibrational velocity vector of the  $\ell^{\text{th}}$  atom  $\vec{v}_{v,\ell}$  is calculated as  $\vec{v}_\ell - \vec{v}_{t,\ell} - \vec{v}_{r,\ell}$ , where  $\vec{v}_\ell$  is the velocity vector of the  $\ell^{\text{th}}$  atom and  $\vec{v}_{r,\ell}$  is the cross product of the angular velocity and the positional vector of the  $\ell^{\text{th}}$  atom relative to the center of the mass of the molecule.

The 2PT model is built upon the hypothesis that the vibrational density of states can be decomposed into gas-like (diffusive) and solid-like (oscillatory) contributions. This simple idea is easily understood based on the ideal gas and the Einstein solid. In the ideal gas, molecular motion is not affected by collisions with neighbors. Thus, the vibrational frequency of the motions in the ideal gas becomes zero in Fourier space. In the Einstein solid, on the other hand, all molecules oscillate with the same non-zero frequency ( $\nu_0$ ). The density of states of the Einstein crystal is represented as a Dirac-delta function  $\Psi(\nu) = \delta(\nu - \nu_0)$ . Real fluids show an intermediate behavior between these two extremes. For instance, the density of states of a dilute gas monotonically decays with an increase in frequency, whereas the density of states in a solid is close to zero at  $\nu = 0$  and shows a broad distribution unlike the Einstein crystal model.

The 2PT model calculates thermodynamic properties by decomposing the density of states of each motion into gas-like and solid-like contributions [Eq. (3)].

$$\Psi^m(\nu) = \Psi_g^m(\nu) + \Psi_s^m(\nu) \quad (m = t, r, \text{ or } v) \quad (3)$$

To decompose  $\Psi^m(\nu)$ , Lin et al.<sup>46</sup> introduced the fluidicity ( $f_g^m$ ), an order parameter to quantify the *gas-likeness* of motions [Eq. (4)].

$$f_g^m = \frac{\int_0^\infty \Psi_g^m(\nu) d\nu}{\int_0^\infty \Psi^m(\nu) d\nu} \quad (4)$$

The fluidicity is calculated from the Carnahan-Starling equation of state<sup>55</sup> (see Lin et al.<sup>42</sup> for the detailed derivation of the fluidicity). Since the integral of the vibrational density of states for each motion equals the degrees of freedom ( $= 3N$ ),  $f_g^m$  can also be seen as the fraction of the degrees of freedom corresponding to gas-like motions.

The contribution of each type of motion to a thermodynamic variable ( $Q^m$ ) is calculated as a sum of the solid-like and gas-like contributions, which is expressed as

$$Q^m = Q_0 + k_B T \int_0^\infty \left[ \Psi_g^m(\nu) W_{Q,g}^m(\nu) + \Psi_s^m(\nu) W_{Q,s}^m(\nu) \right] d\nu \quad (5)$$

where  $Q_0$  is the reference property,  $W_{Q,p}$  ( $p = g$  or  $s$ ) is the weighting function for the gas-like and the solid-like contributions to the property  $Q$ . The reference energy  $E_0$  is defined in Eq. (6).

$$E_0 = E^{\text{MD}} - 3Nk_B T (1 - 0.5f_g^t - 0.5f_r^t) \quad (6)$$

The reference entropy is zero. The weighting functions are given

in Eq. (7).<sup>46</sup>

$$W_{E,g}^t = 0.5 \quad (7a)$$

$$W_{S,g}^t = \frac{1}{3} \left[ \frac{5}{2} + \ln \left( \frac{V}{N f_g \Lambda^3} \right) + \frac{\gamma(3\gamma-4)}{(1-\gamma)^2} \right] \quad (7b)$$

$$W_{A,g}^t = W_{E,g}^t - W_{S,g}^t \quad (7c)$$

$$W_{E,g}^r = 0.5 \quad (7d)$$

$$W_{E,g}^r = \frac{1}{2} + \frac{1}{6} \ln \left( \frac{\pi T^3}{\sigma \Theta^x \Theta^y \Theta^z} \right) \quad (7e)$$

$$W_{A,g}^r = W_{E,g}^r - W_{S,g}^r \quad (7f)$$

$$W_{E,s}^t = W_{E,s}^r = \frac{h\nu}{2k_B T} + \frac{h\nu/k_B T}{\exp(h\nu/k_B T) - 1} \quad (7g)$$

$$W_{S,s}^t = W_{S,s}^r = \frac{h\nu/k_B T}{\exp(h\nu/k_B T) - 1} - \ln \left[ 1 - \exp \left( -\frac{h\nu}{k_B T} \right) \right] \quad (7h)$$

$$W_{A,s}^t = W_{A,s}^r = \ln \left[ \frac{1 - \exp(h\nu/k_B T)}{\exp(-h\nu/2k_B T)} \right] \quad (7i)$$

In Eq. (7),  $h$  is the Planck constant,  $\Lambda$  is the thermal de Broglie wavelength ( $= \sqrt{h^2/2\pi m k_B T}$ ),  $\Theta^k$  ( $k = x, y, \text{ and } z$ ) is the rotational temperature given as  $h^2/8\pi^2 I^k k_B$ ,  $\sigma$  is the rotational symmetry, and  $\gamma$  is the hard sphere volume defined as

$$\gamma = (f_g^t)^{5/2} \left[ \frac{2\Psi^t(0)}{9N} \left( \frac{\pi k_B T}{M} \right)^{1/2} \left( \frac{N}{V} \right)^{1/3} \left( \frac{6}{\pi} \right)^{2/3} \right]^{3/2}. \quad (8)$$

Eq. (7b) is slightly different from the weighting function provided by Lin et al.<sup>46</sup> following the suggestion by Sun et al.<sup>56</sup> The fluidicity of the intramolecular vibration is zero regardless of the thermodynamic conditions ( $f_g^v = 0$ ). The weighting functions for the intramolecular vibrational density of states are identical to the weighting functions for the solid-like translational motions (Eq. 7g-i). Since the TIP4P/2005 model is rigid, the intramolecular vibrational density of states is not calculated in the main article.

After obtaining the internal energy ( $E$ ) and pressure ( $p$ ) from the 2 ns production run and calculating absolute entropy ( $S$ ) based on Eq. (5) and (7), the Gibbs free energy is calculated as  $G = H - TS = E + pV - TS$  where  $H$  is enthalpy ( $H = E + pV$ ).

### 2.3 Velocity autocorrelation criterion

The velocity autocorrelation criterion proposed by Brazhkin et al.<sup>25</sup> defines the FL as the thermodynamic state where the translational velocity autocorrelation function [ $Z(t)$ ] starts to oscillate with decreasing temperature along the isochore.  $Z(t)$  is defined as

$$Z(t) = \frac{1}{3N} \sum_{j=1}^N \sum_{k=1}^3 v_{t,j}^k(t) v_{t,j}^k(0). \quad (9)$$

We define the FL from the  $Z(t)$  criterion as the crossover density where the  $Z(t)$  starts to oscillate with an increase in the bulk density along the isotherm. Fig. 1 shows the behavior of the  $Z(t)$  data normalized by the initial magnitude for different densities at  $T_r = 2.0$ . In order to determine the crossover densities,  $Z(t)$  is first differentiated with regard to time. Then, the lowest density where  $Z(t)$  starts to show a positive slope is computed.

Both  $Z(t)$  and  $\Psi^t(v)$  can be used to calculate the translational

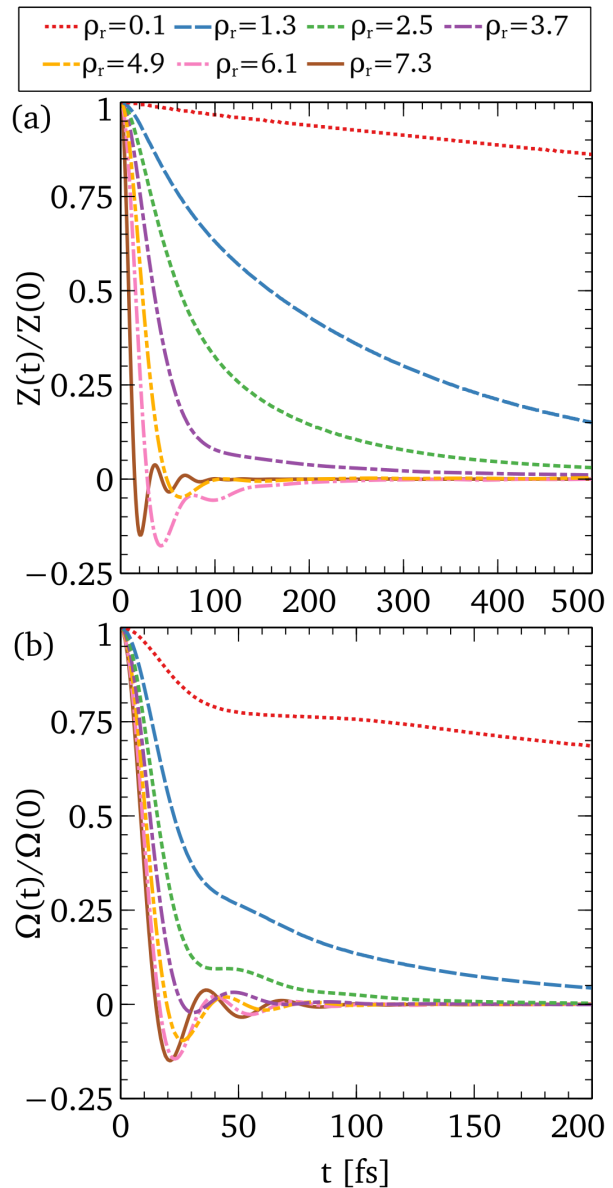


**Fig. 1** (a) Translational and (b) rotational (angular) velocity autocorrelation functions at the temperature of  $T_r = 2.0$ . Colored lines denote different densities. Both autocorrelation functions oscillate when the density increases. The crossover density obtained from the  $Z(t)$  criterion ( $\rho_{cr}^{2PT}$ ) at  $T_r = 2.0$  is  $\rho_{cr}^{2PT} \approx 4.35$ .

diffusion coefficients. The translational diffusion coefficient ( $D_t$ ) is given as:

$$D_t = \frac{1}{3} \int_0^\infty Z(t) dt = \frac{\Psi(0) k_B T}{12MN} \quad (10)$$

For comparison, we also calculate the angular velocity autocorrelation function ( $\Omega(t)$ ), which is defined in a similar manner.

$$\Omega(t) = \frac{1}{3N} \sum_{j=1}^N \sum_{k=1}^3 \omega_j^k(t) \omega_j^k(0) \quad (11)$$

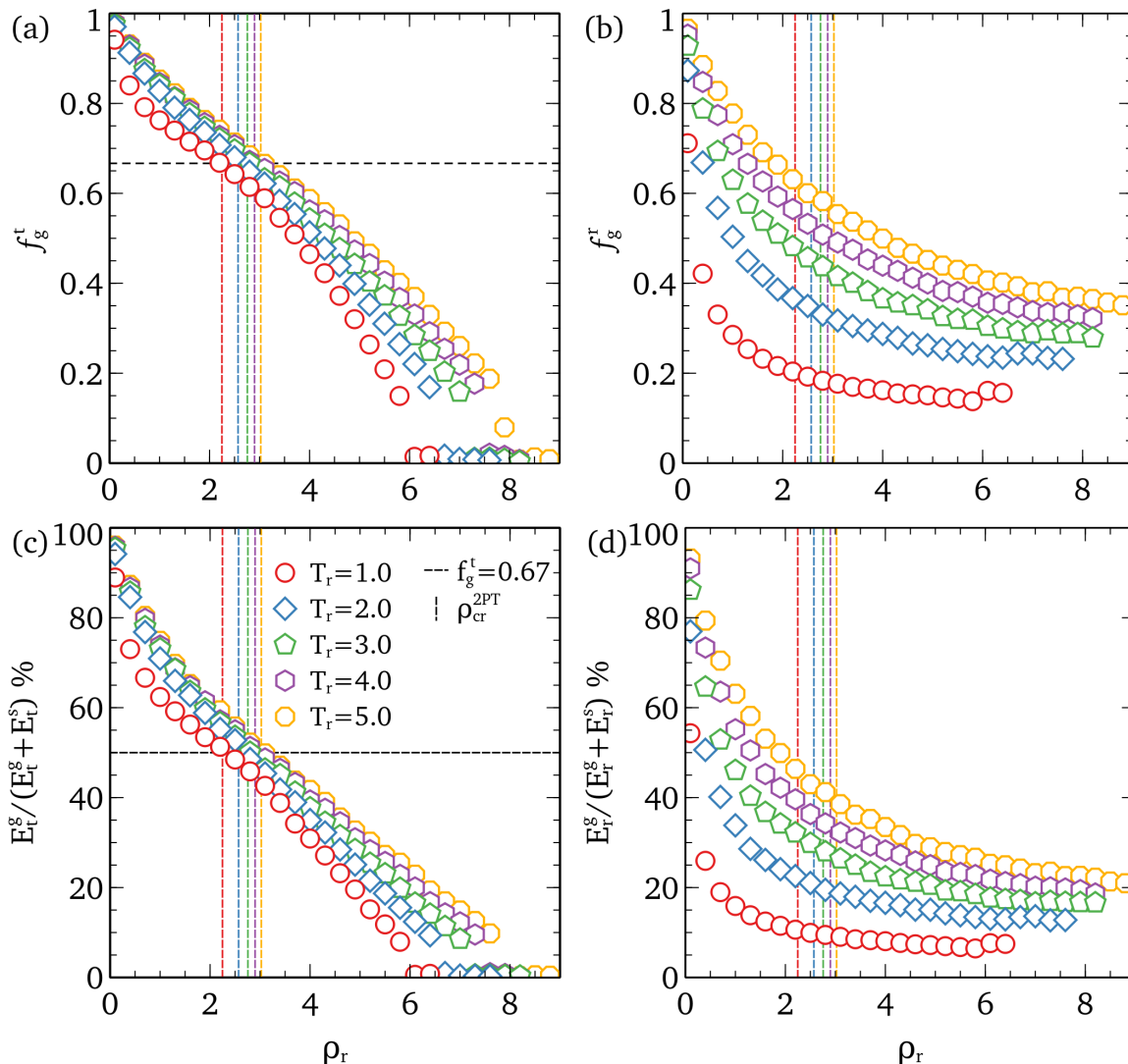


**Fig. 2** (a) Translational fluidicity ( $f_g^t$ ) and (b) rotational fluidicity ( $f_g^r$ ) of the TIP4P/2005 water model along isotherms.  $f_g^t$  has its inflection density in the vicinity of  $f_g^t = 0.67$  (horizontal dashed line). (c) and (d) show the percent of gas-like (diffusive) contribution to translational and rotational energy, respectively. The translational energy contribution of gas-like fraction becomes equal to that of solid-like fraction [ $E_r^g = E_r^s$ , black dashed line in (c)] when  $f_g^t$  becomes 0.67. The vertical colored lines are drawn to indicate the densities where  $E_r^g/(E_r^g + E_r^s)$  becomes 50 %.

## 2.4 Estimation of the melting density

We use both  $NVT$  and  $NpT$  results to locate the solid-liquid coexistence line. In the  $NVT$  simulations, the solid-liquid transition pressure is determined by examining the abrupt changes in the fluidicity, Gibbs (or Helmholtz) free energy, and pressure along an isotherm. The translational fluidicity, for instance, abruptly decreases to zero when the solid-liquid transition occurs (see Fig. 2). From the pressure data, the solid-liquid transition pressure can be obtained by fitting two polynomial equations in the vicinity of the transition point and finding the pressure where the fitted equations become equal.

In the  $NpT$  simulations, the coexistence densities are determined by examining thermodynamic variables. The melting temperature and densities are estimated as the point where the thermodynamic variables show an abrupt change.

## 2.5 Structural analysis

We examine the structural characteristics by analyzing the trajectory data obtained from the  $NVT$  simulations ( $N = 2,000$ ). The number of hydrogen bonds (HB) per molecule ( $\langle n_{HB} \rangle$ ), the orientational tetrahedral order parameter ( $\langle \langle q \rangle \rangle$ )<sup>57,58</sup>, and the topological characteristics of Voronoi cells are computed.

We use two HB definitions,<sup>59–61</sup> which are denoted as E (electronic structure criterion) and G (geometric criterion). The electronic structure based definition<sup>59</sup> deems two molecules to be hydrogen bonded if the following condition is satisfied.

$$\exp\left(-\frac{r_{O\dots O}}{0.343}\right)\left(7.1 - 0.050\psi + 0.00021\psi^2\right) > 0.0085 \quad (12)$$

In Eq. (12),  $r_{O\dots O}$  is the intermolecular distance ( $\text{\AA}$ ) between the two O atoms and  $\psi$  ( $^\circ$ ) is the angle between the OH vector and a normal vector to a plane passing through all atoms in the donor molecule. The geometric definition uses four criteria sug-

gested by the two previous works.<sup>60,61</sup> Himoto et al.<sup>60</sup> regard two molecules to be hydrogen bonded if the intermolecular OH distance ( $r_{O\dots H}$ ) is shorter than 2.2 Å and the angle between the intramolecular OH vector ( $\vec{r}_{OH}$ ) and the intermolecular OH vector ( $\vec{r}_{O\dots H}$ ) is less than 30°. Based on the *ab initio* MD simulations, Pan et al.<sup>61</sup> suggest that  $r_{O\dots H}$  and  $r_{H\dots H}$  should be longer than 1.62 Å and 2 Å reflecting strong repulsive interactions. For both definitions, the numbers of HBs per molecule are computed as<sup>13</sup>

$$\langle n_{\text{HB}} \rangle = \frac{\sum_{i=1}^N b_{ij}}{N} \quad (13)$$

where  $b_{ij}$  is unity if the molecules  $i$  and  $j$  are hydrogen-bonded. Otherwise, it is zero.

The orientational tetrahedral order parameter is defined as

$$q_k = 1 - \frac{3}{8} \sum_{i=1}^3 \sum_{j=i+1}^4 \left( \cos \theta_{ikj} + \frac{1}{3} \right)^2, \quad (14)$$

where  $\theta_{ikj}$  is the angle between the molecule  $k$  and two of its four nearest neighbors  $i$  and  $j$ . The average of  $q_k$  ( $\langle q \rangle = \sum_{k=1}^N q_k / N$ ) is zero for an ideal gas and unity for perfectly tetrahedral structures.<sup>57,58</sup>

Aragones et al.<sup>44</sup> identify two crystalline structures at high temperature and pressure, namely, the body-centered cubic (BCC) and the face-centered cubic (FCC) depending on the thermodynamic conditions. The BCC structure becomes unstable relative to FCC at high temperatures. We expect that the local structure of supercritical water will show signs of solidification before it freezes. This precursor to solidification can be studied by exploiting the topological information at the molecular level. We use the code *VoroTop* (developed by Lazar et al.<sup>62</sup>) to obtain the topological information, which has been successfully used for the characterization of simple fluid models.<sup>31,39,63</sup>

In this framework, a configuration of  $N$  particles is partitioned into the  $N$  Voronoi cells, which are defined as the region in space closer to the central particle than any other neighbors. The shape of a Voronoi cell contains the connectivity information for the central molecule (atom) and its surrounding neighbors. This topological type of Voronoi cell can be completely encoded into a Weinberg vector.<sup>64</sup> The Weinberg vector can be generated by reading the Schlegel diagram of a Voronoi cell,<sup>65</sup> a projection of the three-dimensional polyhedron to a two-dimensional graph. After the Weinberg vectors of a system are obtained, they are compared to the topological types found in a variety of crystalline structures (e.g., face-centered cubic (FCC), body-centered cubic (BCC), hexagonal closed packed (HCP), etc.). For the detailed description on the algorithm, see Lazar et al.<sup>62</sup>

### 3 Results and Discussion

Fig. 1 shows the translational velocity and the angular velocity autocorrelation functions [ $Z(t)$  and  $\Omega(t)$ ] normalized by their initial intensity. As Brazhkin et al. noted,<sup>25</sup> the translational velocity autocorrelation function  $Z(t)$  starts to oscillate with an increase in density. The dynamic crossover densities [ $\rho_{\text{cr}}^{Z(t)}$ ] are obtained based on the procedure described in Sec. 2.3. The crossover densities agree well with those obtained by previous works (see Fig.

4).<sup>20,21</sup> This result suggests that the FL characterized by the  $Z(t)$  criterion is not path-dependent unlike the Widom line defined based on the maxima of thermodynamic response functions.<sup>14</sup> Compared to  $Z(t)$ ,  $\Omega(t)$  becomes oscillatory at lower densities [see Fig. 1 (b)]. The onset of the oscillatory behavior in  $\Omega(t)$  at low density reflects that the rotational motion of a molecule is more sensitive to the presence of neighboring molecules. The translational motion of a molecule becomes oscillatory only when the molecule is effectively arrested by its neighbors, which is also known as the cage effect in cell theory. On the other hand, the rotational motion can be easily restricted by the presence of its neighboring molecules. Since water is an associating fluid, cluster formation readily occurs in the gas-like domain,<sup>16</sup> which results in the oscillation of  $\Omega(t)$  at lower density.

Fig. 2 (a) shows how the translational fluidicity ( $f_{\text{g}}^t$ ) changes as the density increases along an isotherm.  $f_{\text{g}}^t$  does not decrease linearly with an increase of the density. Instead, an inflection occurs at  $f_{\text{g}}^t \sim 0.67$  at all simulation temperatures. The inflection point can be located by fitting an empirical two-term exponential function to the fluidicity data in the fluid region as shown in our previous work.<sup>32</sup> It also shows an abrupt decrease to zero at high density, which implies solidification.

The inflection of the fluidicity at  $f_{\text{g}}^t \sim 0.67$  aligns with the heat capacity criterion proposed by Brazhkin and his coworkers<sup>24</sup> to some extent. The heat capacity criterion states that the FL is a collection of thermodynamic states where the heat capacity becomes  $6.0 k_{\text{B}}$  for water.<sup>20,21</sup> The connection between the fluidicity and the heat capacity can be clarified as follows.<sup>32</sup> The heat capacity of a monatomic ideal gas is  $1.5 k_{\text{B}}$ , and that of Einstein crystal is given in Eq. (15).

$$C_v = 3k_{\text{B}} \left( \frac{h\nu_0}{k_{\text{B}}T} \right)^2 \frac{\exp(h\nu_0/k_{\text{B}}T)}{[\exp(h\nu_0/k_{\text{B}}T) - 1]^2} \quad (15)$$

At the high temperature limit ( $T \rightarrow \infty$ ), Eq. (15) converges to  $3 k_{\text{B}}$ .<sup>66</sup> Taking into account that the heat capacity is proportional to the degrees of freedom, the translational contribution to the heat capacity in the high temperature limit is

$$\lim_{T \rightarrow \infty} C_v^t(T) = \frac{2}{3} (1.5k_{\text{B}}) + \frac{1}{3} (3k_{\text{B}}) = 2k_{\text{B}} \quad (16)$$

for a monatomic system. Since water consists of three atoms, the translational contribution to the total heat capacity is obtained as  $6k_{\text{B}}$  at the temperature limit. However, it should be noted that the above derivation has several limitations. First, the rotational contribution to the heat capacity is not included ( $C_v \neq C_v^t$ ). Second, this relation holds exactly at the high temperature limit. Lastly, the Einstein model is a simple monatomic model that does not consider the distribution of vibrational frequencies. This may provide a partial explanation for the inconsistency of the thermodynamic and dynamic criteria as denoted by Fomin et al.<sup>21</sup>

The density dependence of the rotational fluidicity ( $f_{\text{g}}^r$ ) is dissimilar to that of the translational fluidicity [Fig. 2 (b)]. It quickly converges to its minimum as the density decreases but does not become zero. As shown in Fig. 1 (b), the convergence behavior of the rotational fluidicity reflects that it is not relevant to the FL.

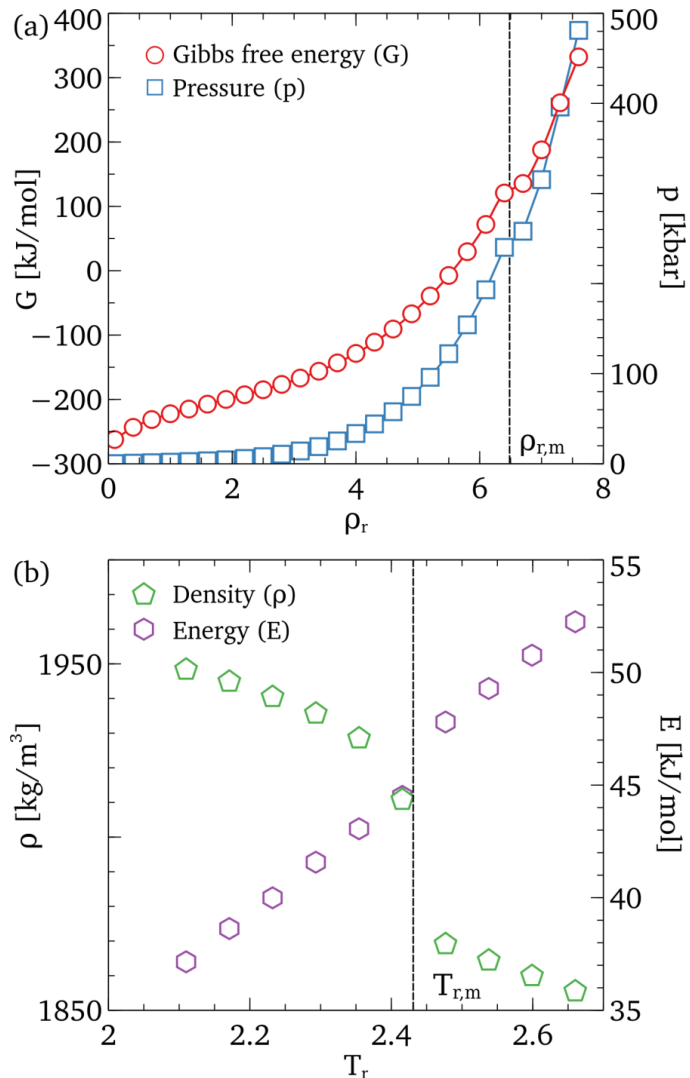


**Fig. 3** (a) Gibbs free energy (G) and pressure (p) of supercritical water (TIP4P/2005) along an isotherm ( $T_r = 2.0$ ). Both G and p shows a discontinuity at the density around  $\rho_r = 6.49$ . (b) Energy (E) and density ( $\rho$ ) along an isobar ( $p = 300$  kbar). Both E and  $\rho$  shows an abrupt change across the melting temperature [ $T_m = 1590.25$  K ( $T_{r,m} \sim 2.43$ )].

The non-zero rotational fluidicity in the ice region reflects that supercritical water transforms not to ice VII but to a plastic crystal (PC).

Fig. 2 (c) and (d) shows the gas-like contribution to the translational and rotational energy. The gas-like translational energy becomes equal to the solid-like contribution at the point where the translational fluidicity becomes 0.67, and then decreases to zero at the solid-liquid transition point. However, the gas-like rotational energy does not converge to zero but its contribution increases with an increase in the temperature. All these results suggest that the translational dynamic crossover of supercritical water can be identified using the 2PT model, as was shown for simple fluids.<sup>32</sup>

Fig. 3 (a) shows the pressure and enthalpy of the TIP4P/2005 water model along an isotherm ( $T_r = 2.0$ ). The Gibbs free energy and the pressure show an abrupt change near  $\rho_r = 6.49$ , which

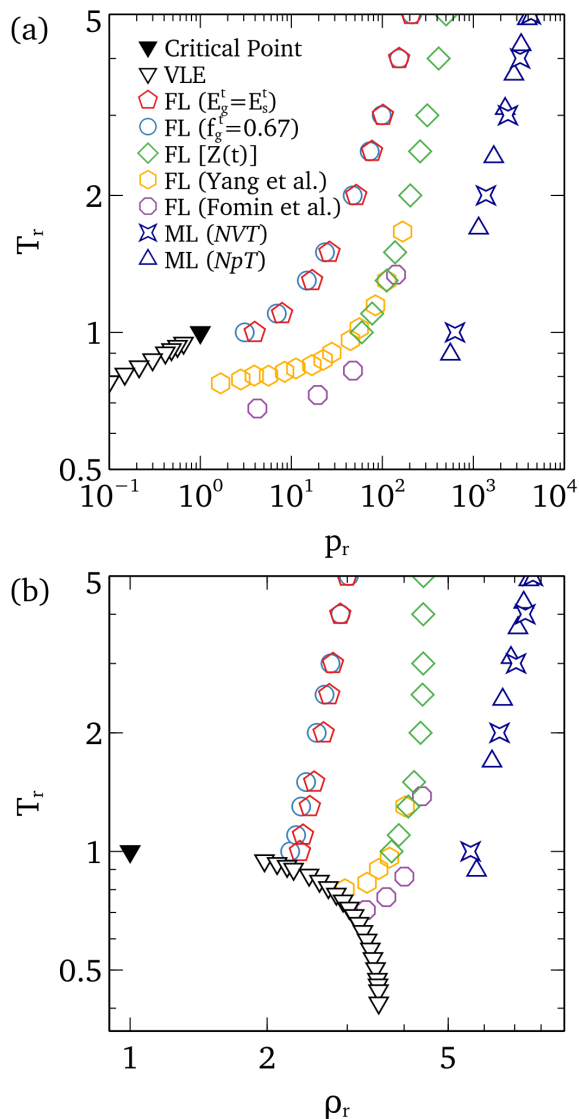


**Fig. 4** (a)  $p_r - T_r$  diagram and (b)  $\rho_r - T_r$  diagrams of supercritical water (TIP4P/2005). The critical point and the VLE lines are from previous works.<sup>16,20,21,67</sup> The MLs obtained from different methods are consistent with each other. In (b), only the liquid density at the solid-liquid coexistence line is presented. The FLs determined by  $Z(t)$  criterion agree with previous works.<sup>20,21</sup> The FLs from the 2PT model agree well with each other and run parallel to the ML but they do not agree with the FL defined by the  $Z(t)$  criterion.

agrees well with the abrupt change in the translational and rotational fluidicities as shown in Fig. 2. Fig. 3 (b) shows the density ( $\rho$ ) and the internal energy (E) change along an isobar ( $p = 300$  kbar). Both thermodynamic variables show an almost linear dependence on the temperature far from the melting temperature ( $T_{r,m} \sim 2.45$ ). The melting temperature and the coexistence densities thus can be estimated from the abrupt change.

Fig. 4 compares the FLs in supercritical water from the 2PT criteria ( $f_g^t = 0.67$  and  $E_g^t = E_s^t$ ) to that obtained using the  $Z(t)$  criterion. The FLs from the 2PT criteria are consistent with each other and run parallel to the MLs, like those of simple fluids.

The MLs obtained from the  $NVT$  simulations and  $NpT$  simulations agree well with each other, which validates our hypothesis that the solid-liquid transition in high-temperature water is dominated by the short-range attractive and repulsive interactions. However, the FLs obtained using the 2PT model do not agree with that defined by the  $Z(t)$  criterion. The slope of the  $Z(t)$  criterion FL is not parallel to the melting line in both  $p - T$  and  $\rho - T$  planes, which is at odds with the expectation proposed by Fomin et al.<sup>21</sup> When a power law equation ( $T_r = a\rho_r^b$  where  $a$  and  $b$  are fitting parameters) is fitted, the slope of the ML is obtained as  $5.502 \pm 0.055$ . The slope of the FL from the 2PT method is  $5.482 \pm 0.071$ , whereas that from the  $Z(t)$  criterion could not be fitted to a simple power law equation. The crossover densities from the  $Z(t)$  criterion become almost identical regardless of the temperature above  $T_r = 2.0$  as shown by Fomin et al.<sup>21</sup> The disagreement of the crossover densities from the 2PT model and the  $Z(t)$  criteria is seemingly paradoxical since the density of states is merely obtained by converting  $Z(t)$  from the time domain to the frequency domain following the Wiener-Khinchin theorem.<sup>42</sup>

In order to understand how this inconsistency occurs, we compute the solid-like translational density of states ( $\Psi_s^t$ ) in ambient water (Fig. 5a). Regardless of how the FL is defined, ambient water ( $\rho_r = 3.52$  and  $T_r = 0.46$ ) is classified as a rigid (solid-like) liquid. Unlike a simple Lennard-Jones fluid,<sup>32,42</sup> there are two distinct vibrational modes present in ambient water. The right-skewed low-frequency mode at  $50 \text{ cm}^{-1}$  originates from the bending of hydrogen bonds (HBs), whereas that at  $200 \text{ cm}^{-1}$  is associated with the intermolecular collisions in the first coordination shell. These two types of oscillatory motions have been reported in both ambient and supercooled water.<sup>68–70</sup>  $\Psi_s^t(\nu)$  in supercritical water is unimodal but its skewness changes with increasing density in the fluid region. After its transition to the PC, two distinct modes are again observed. Taking into account the distinct peaks observed in ambient water, the peak broadening and the skewness change in  $\Psi_s^t$  suggest that the unimodal  $\Psi_s^t$  could be the result of a superposition of the two modes that represent the different types of underlying oscillations.

The presence of dissimilar vibrations provides an insight into the inconsistency between the FLs obtained from the 2PT model and  $Z(t)$ . The  $Z(t)$  criterion focuses on the occurrence of the high-frequency oscillation in  $Z(t)$ , which arises from collisions inside the first coordination shell. Only the high-frequency mode is easily observable when examining the oscillatory behavior of  $Z(t)$ . On the other hand, the 2PT model calculates the solid-like contribution by subtracting the gas-like translational density of states from the translational density of states; the 2PT method assumes that both oscillatory modes contribute to the solid-like behavior of water molecules. Considering the two different vibrational modes observed in ambient water and the parallelism between the melting line and the FL observed in a variety of model fluids,<sup>25,63</sup> the FL obtained from the 2PT model is closer to the original notion of the Frenkel line.

We interrogate how these two oscillatory modes are related to the dynamic and structural characteristics of supercritical water. Fig. 6 (a) shows that the translational diffusion coefficient qualitatively changes across the crossover densities obtained from both

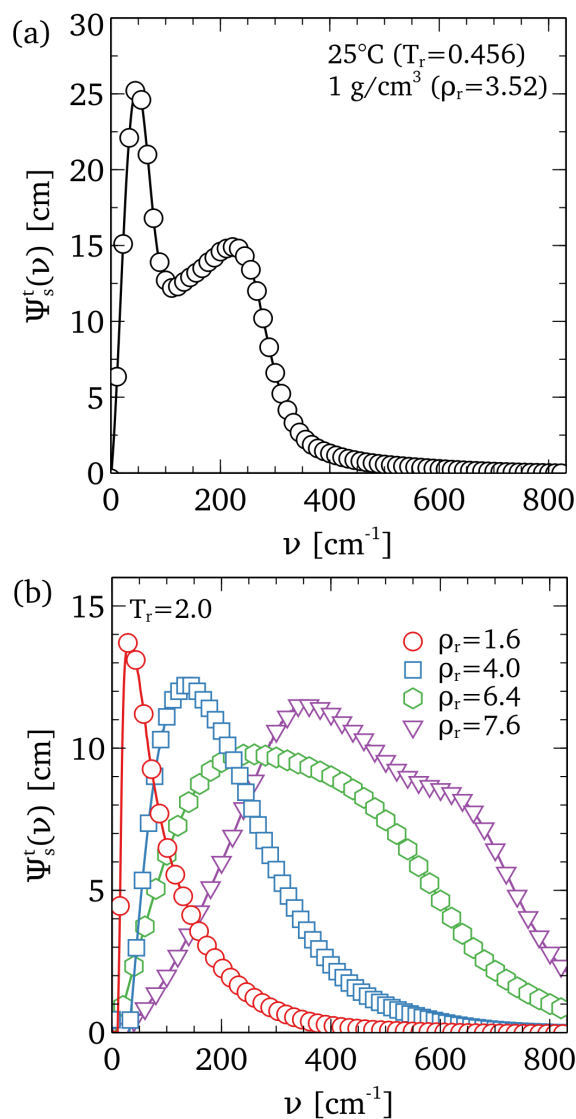


**Fig. 5** Solid-like contribution to the vibrational density of states of translational motions [ $\Psi_s^t(\nu)$ ] at (a) ambient condition (298 K,  $1.0 \text{ g/cm}^3$ ) and (b)  $T_r = 2.0$  over a range of densities.  $\Psi_s^t(\nu)$  in rigid liquid (ambient water) shows two distinct modes, which suggests the presence of the solid-like dynamic heterogeneity in water. As the density increases along an isotherm in the fluid region,  $\Psi_s^t$  is broadened and becomes less skewed. After its transition to the plastic crystal (PC,  $\rho_r = 7.6$ ), two vibrational modes are again observed.

the 2PT model and the  $Z(t)$  criterion. The logarithm of  $D_t$  decreases steeply in the low-density region. Then, it decreases linearly between the two FLs and again declines steeply across the FL obtained from the  $Z(t)$  criterion. These quantitatively different dependencies on bulk density support the idea that different oscillatory motions exist in the near-critical region. The low-frequency vibrational contribution related to HB bending, however, fades with increasing temperature due to the vigorous thermal motions.

As shown in the  $\rho_r - T_r$  diagram [Fig. 4 (b)], the FL from the 2PT criterion and the ML can be fitted to a power law equation ( $T_r = a\rho_r^b$  where  $b \approx 5.5$ ). That is, the FL from the 2PT model at

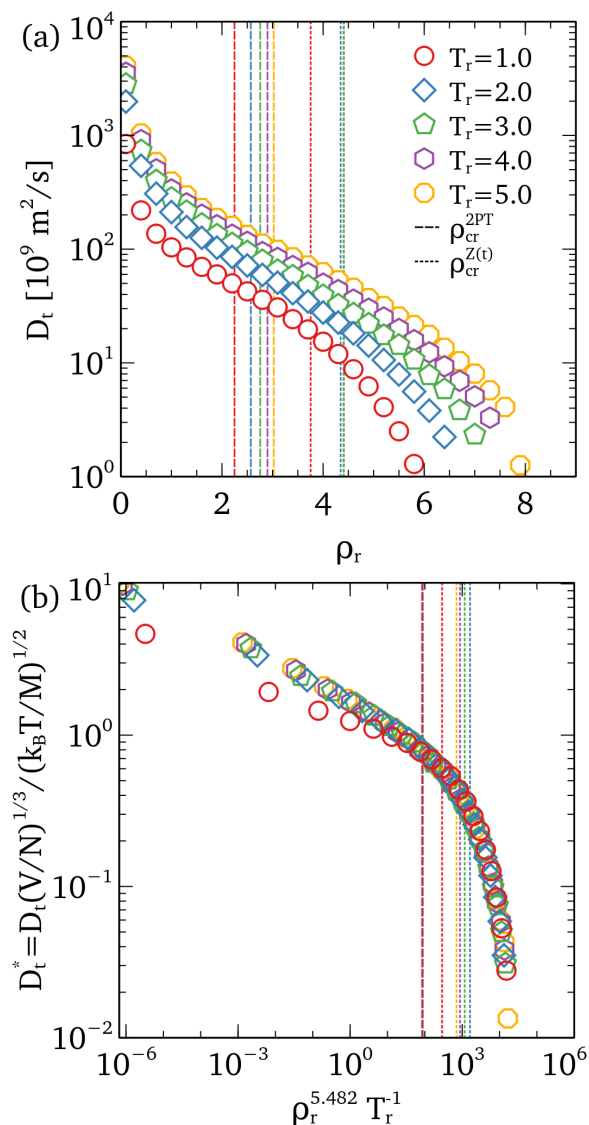


**Fig. 6** (a) Translational diffusion coefficients ( $D_t$ ) as a function of the bulk density. Note the qualitative changes across the crossover densities from the two different criteria (2PT, dashed lines and  $Z(t)$ , dotted lines). (b) Test of thermodynamic scaling of the translational diffusion coefficients. All dimensionless diffusivity curves collapse to a single line above the crossover densities from the 2PT criterion (dashed lines).

different thermodynamic conditions can be collapsed as a single point ( $\rho_r^{5.5}/T_r \approx \text{constant}$ ). This density scaling scenario is tested by defining the reduced translational diffusivity, which is given as:<sup>38</sup>

$$D_t^* = D_t \frac{(V/N)^{1/3}}{(k_B T/M)^{1/2}} \quad (17)$$

Fig. 6 (b) shows the thermodynamic scaling result. All  $D_t^*$  curves collapse to a single curve in the region between the FL from the 2PT criterion and the ML. When the temperature is above  $T_r = 2.0$ , the curves become close to each other even when the density is much lower than the crossover densities, which can be understood as a result of the competition between the hydrogen bonding and the thermal motion. The collapse of  $D_t^*$  unambiguously

reveals the physical meaning of the FL from the 2PT criteria; it is a set of the lowest densities where the power-law density scaling holds in supercritical water. On the other hand, the density scaling is not successful when the FL from the  $Z(t)$  criterion is used since it cannot be fitted to the power-law relation.

Fig. 7 (a) shows the number of hydrogen bonds (HBs) per molecule from the electronic structure definition ( $\langle n_{\text{HB}}^{\text{E}} \rangle$ ).<sup>59</sup>  $\langle n_{\text{HB}}^{\text{E}} \rangle$  shows an inflection in the vicinity of the critical temperature but it quickly collapses to a single line above  $T_r > 2$ . It becomes larger than four at very high densities ( $\rho_r > 6.0$ ), which is seemingly unphysical. In contrast, the HB number per molecule obtained from the geometric criterion [ $\langle n_{\text{HB}}^{\text{G}} \rangle$ , Fig. 7 (b)] is always below three at all studied temperatures. It reaches a maximum along the isotherm in the fluid state, which suggests that the hydrogen bond formation is hampered at high densities due to repulsive interactions.<sup>61,71</sup> Together with the emergence of the slow vibrational mode observed in Fig. 5 (b), the abrupt increase in  $\langle n_{\text{HB}}^{\text{G}} \rangle$  would indicate the solid-liquid transition. Overall, the geometric criterion is more coincident with the dynamic interpretation than is the electron energy criterion. It would be instructive to understand how the seemingly unphysical number of HBs is obtained. When only a single distance criterion ( $r_{\text{O...H}} < 2.2 \text{ \AA}$ ) is used to define the hydrogen bond ( $\langle n_{\text{HB}}^{\text{G}'} \rangle$ ), the overall behavior becomes similar to that of  $\langle n_{\text{HB}}^{\text{E}} \rangle$  [see Fig. S1 in the ESI<sup>†</sup>]. The addition of the lower limits proposed by Pan et al.<sup>61</sup> slightly decreases  $\langle n_{\text{HB}}^{\text{G}} \rangle$  at high density, but the result is not largely different from  $\langle n_{\text{HB}}^{\text{E}} \rangle$ . These results indicate that the addition of the angle criterion ( $\angle_{\text{OH...O}} < 30^\circ$ ) is the reason for the discrepancy.

Orientalional (topological) characteristics are quantitatively analyzed by the orientational tetrahedral order parameter and the variation in the topological types. The orientational order parameter ( $\langle q \rangle$ ) steeply increases with an increase of the density in the gas-like domain [Fig. 8 (a)]. It becomes concave downward at the crossover densities from the 2PT model ( $\rho_{\text{cr}}^{2\text{PT}}$ ), and shows a maximum around those from the  $Z(t)$  criterion. In the vicinity of the solid-liquid transition, it becomes discontinuous. This result suggests that the tetrahedral structure of water is weakened in dense supercritical water between the FL and the ML. As the temperature increases, the vigorous thermal motion of the water molecules breaks down the hydrogen bonding network and  $\langle q \rangle_{\text{max}}$  decreases as shown in Fig. 7 (b). Water becomes more similar to *simple fluids without tetrahedral order*<sup>38</sup> and the two crossover densities approach each other (see Fig. 4).

In the topological analysis, only small fractions of body-centered cubic (BCC) or icosahedral types ( $< 0.01\%$ ) are observed at all state points. Rather, most Voronoi cells in the PC are classified as the topological types that are found in the face-centered cubic (FCC) and hexagonal closest packed (HCP) structures as obtained by Aragonés et al.<sup>44</sup> [see Fig. 8 (b)]. In the low density region, the fraction of the FCC-HCP topological types ( $f_{\text{FCC-HCP}}$ ) linearly increases with an increase of the density. At the density above  $\rho_{\text{cr}}^{2\text{PT}}$ , the slope of the  $f_{\text{FCC-HCP}}$  curve starts to increase, and becomes again linear above  $\rho_{\text{cr}}^{Z(t)}$ . Thus, the tetrahedral order parameter and the topological characteristics reflect the dynamic crossover of supercritical water across the Frenkel lines.

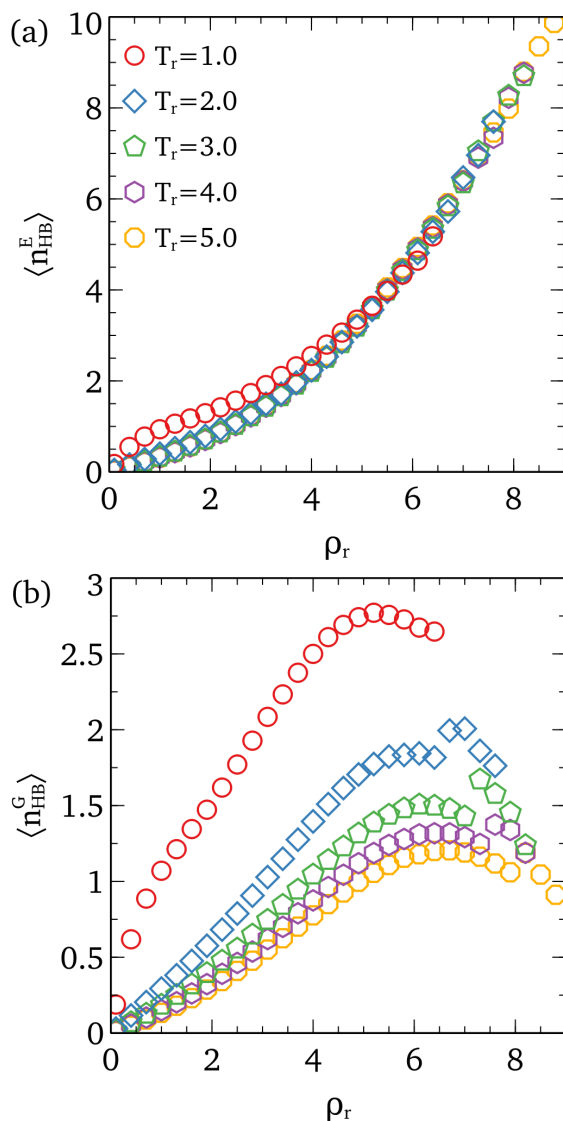


**Fig. 7** The average number of hydrogen bonds (HBs) per water molecule defined by (a) the electron energy criterion (E) and (b) the geometric criterion (G).  $\langle n_{\text{HB}}^{\text{E}} \rangle$  monotonically increases and becomes beyond four in the high density region. On the other hand,  $\langle n_{\text{HB}}^{\text{G}} \rangle$  is less than four and shows a maximum near the solid-liquid transition density.

## 4 Conclusions

Overall analyses suggest that the Frenkel line from the two-phase thermodynamic method and that from the velocity autocorrelation criterion are related but not identical. Due to the tetrahedral nature of water, the solid-like dynamics of water are not the same as those of simple fluids. There are two distinct oscillatory modes observed in ambient water that would arise from the bending of the hydrogen bonds (long-range attractive interaction) and the cage effect in the first coordination shell (short-range repulsive interaction). The Frenkel lines defined by the 2PT model and the high-frequency oscillation in the  $Z(t)$  function enclose the transition region where the diffusion coefficient decreases exponentially with an increase of the density. Since the 2PT model con-

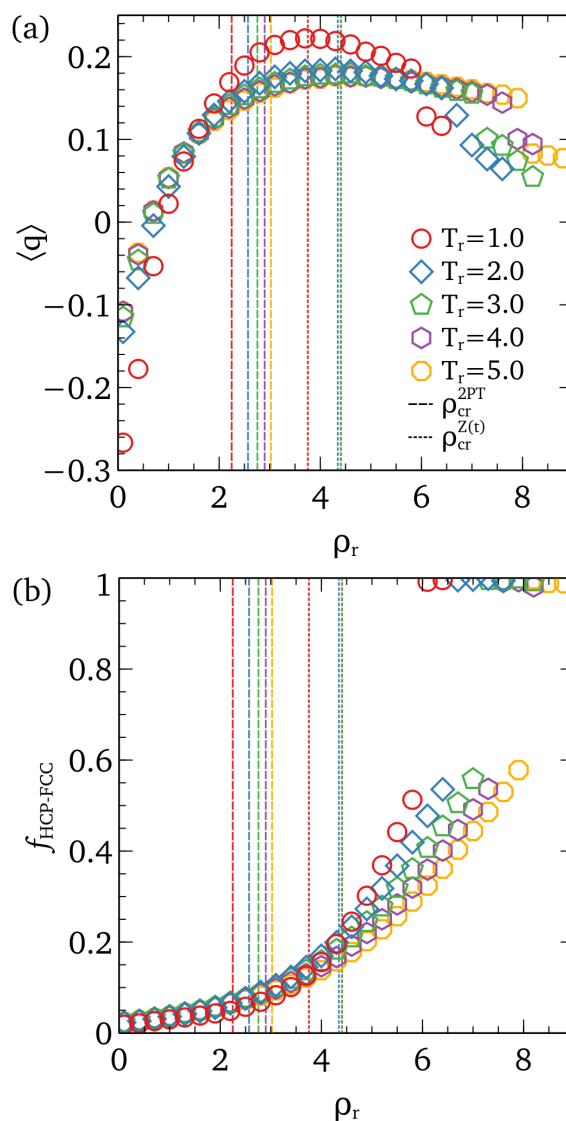


**Fig. 8** (a) The average orientational tetrahedral order parameter ( $\langle q \rangle$ ) and (b) the fraction of FCC and HCP types as a function of the density along isotherms from  $T_r = 1.0$  to  $T_r = 5.0$ .  $\langle q \rangle$  shows its maximum near the crossover densities obtained from the  $Z(t)$  criterion (vertical dotted lines) and becomes discontinuous near the solid-liquid transition densities ( $\rho_r \geq 6$ ). The fraction of FCC/HCP types starts to increase steeply when the bulk density is larger than the crossover densities, and becomes unity at the solid-liquid transition density.

siders both modes from the bending of the hydrogen bonds and collisions within the first coordination shell, the Frenkel line from the 2PT criteria runs parallel to the melting line on the double-logarithmic  $\rho - T$  and  $p - T$  diagrams. The parallelism between the Frenkel line from the two-phase thermodynamic model and the melting line suggests that the thermodynamic scaling relation is obeyed in the region between these lines. On the other hand, the Frenkel line from the  $Z(t)$  criterion characterizes the density where there is a strong confinement induced by repulsive forces. Thus, both Frenkel lines have their own physical meaning. However, the dynamic crossover line from the two-phase thermo-

dynamic model seems closer to the original notion of the Frenkel line due to the two pronounced non-zero frequency modes in ambient water (rigid liquid) and the parallelism of the FL to the melting line.

As Frenkel and Brazhkin et al. originally proposed, and the results obtained in this work demonstrate, the notion of the Frenkel line can be associated with a nonrigid (gas-like, diffusive) to rigid (solid-like, oscillatory) transition. However, it is not directly related to the gas-liquid transition for the following reasons. The Frenkel line unambiguously exists in the hard sphere fluid system where no first-order gas-liquid phase transition exists.<sup>31,32</sup> Thermodynamic properties also show that no high-order phase transition occurs across the FL. Therefore, it would be more appropriate to refer to the FL as a rigid-nonrigid crossover line directly related to the dynamic duality of liquids.

## Conflicts of interest

There are no conflicts to declare.

## Acknowledgements

This work was supported by the Director's Postdoctoral Fellow Program (20190653PRD4) and the Laboratory Directed Research and Development Program (20190057DR) at Los Alamos National Laboratory.

## Notes and references

- J. W. Tester, H. R. Holgate, F. J. Armellini, P. A. Webley, W. R. Killilea, G. T. Hong and H. E. Barner, *Supercritical water oxidation technology: process development and fundamental research*, ACS Publications, 1993.
- T. Adschiri, Y. Hakuta, K. Sue and K. Arai, *J. Nanopart. Res.*, 2001, **3**, 227–235.
- N. G. Holm and E. Andersson, *Astrobiology*, 2005, **5**, 444–460.
- S. Deguchi and K. Tsujii, *Soft Matter*, 2007, **3**, 797–803.
- G. Galli and D. Pan, *Proc. Natl. Acad. Sci. U. S. A.*, 2013, **110**, 6250–6251.
- B. Journaux, K. Kalousová, C. Sotin, G. Tobie, S. Vance, J. Saur, O. Bollengier, L. Noack, T. Rückriemen-Bez, T. Van Hoolst et al., *Space Sci. Rev.*, 2020, **216**, 7.
- S. O. Odu, A. G. van der Ham, S. Metz and S. R. Kersten, *Ind. Eng. Chem. Res.*, 2015, **54**, 5527–5535.
- Y. H. Shin, N. C. Shin, B. Veriansyah, J. Kim and Y.-W. Lee, *J. Hazard. Mater.*, 2009, **163**, 1142–1147.
- A. A. Chialvo and P. T. Cummings, *J. Chem. Phys.*, 1994, **101**, 4466–4469.
- A. G. Kalinichev, *J. Mol. Liq.*, 2017, **241**, 1038–1043.
- G. Simeoni, T. Bryk, F. Gorelli, M. Krisch, G. Ruocco, M. Santoro and T. Scopigno, *Nat. Phys.*, 2010, **6**, 503–507.
- K. Karalis, C. Ludwig and B. Niceno, *Sci. Rep.*, 2019, **9**, 1–10.
- S. E. Strong, L. Shi and J. Skinner, *J. Chem. Phys.*, 2018, **149**, 084504.
- P. Schienbein and D. Marx, *Phys. Rev. E*, 2018, **98**, 022104.
- P. Gallo, D. Corradini and M. Rovere, *Nat. Commun.*, 2014, **5**, 1–6.
- T. J. Yoon, M. Y. Ha, W. B. Lee and Y.-W. Lee, *J. Chem. Phys.*, 2019, **150**, 154503.
- E. A. Ploetz and P. E. Smith, *J. Phys. Chem. B*, 2019, **123**, 6554–6563.
- I. Zerón, J. Torres-Arenas, E. de Jesús, B. Ramírez and A. Benavides, *J. Mol. Liq.*, 2019, **293**, 111518.
- The notion of pseudo-boiling or a supercritical gas-liquid transition was introduced by the pioneering work of Simeoni et al.<sup>11</sup>, and has been actively discussed in the follow-up studies by several authors.<sup>12–16</sup> Similar to the Frenkel line, the notion of a supercritical gas-liquid transition is not completely settled; however, recent works from different theoretical points of view suggest that the introduction of a transition region (not the *Widom line*) integrates the classical idea of a continuous transition into the demarcation of the supercritical fluid region.<sup>16–18</sup> The same philosophy was introduced by the authors.<sup>31</sup> However, since the discussion of the relationship between the supercritical gas-liquid transition and the Frenkel line is beyond the scope of this work, we limit our discussion to the definition of the Frenkel line.
- C. Yang, V. Brazhkin, M. Dove and K. Trachenko, *Phys. Rev. E*, 2015, **91**, 012112.
- Y. D. Fomin, V. Ryzhov, E. Tsiok and V. Brazhkin, *Sci. Rep.*, 2015, **5**, 14234.
- J.-P. Hansen and I. R. McDonald, *Theory of simple liquids*, Academic Press, Amsterdam, The Netherlands, 4th edn., 2013.
- Y. D. Fomin, V. Ryzhov, E. Tsiok, J. Proctor, C. Prescher, V. Prakapenka, K. Trachenko and V. Brazhkin, *J. Phys. Condens. Matter*, 2018, **30**, 134003.
- V. Brazhkin, Y. D. Fomin, A. Lyapin, V. Ryzhov and K. Trachenko, *Phys. Rev. E*, 2012, **85**, 031203.
- V. Brazhkin, Y. D. Fomin, A. Lyapin, V. Ryzhov, E. Tsiok and K. Trachenko, *Phys. Rev. Lett.*, 2013, **111**, 145901.
- T. Bryk, F. Gorelli, I. Mryglod, G. Ruocco, M. Santoro and T. Scopigno, *J. Phys. Chem. Lett.*, 2017, **8**, 4995–5001.
- V. V. Brazhkin, C. Prescher, Y. D. Fomin, E. N. Tsiok, A. G. Lyapin, V. N. Ryzhov, V. B. Prakapenka, J. Stefanski, K. Trachenko and A. Sapelkin, *J. Phys. Chem. B*, 2018, **122**, 6124–6128.
- T. Bryk, F. Gorelli, I. Mryglod, G. Ruocco, M. Santoro and T. Scopigno, *J. Phys. Chem. B*, 2018, **122**, 6120–6123.
- N. P. Kryuchkov, L. A. Mistryukova, V. V. Brazhkin and S. O. Yurchenko, *Sci. Rep.*, 2019, **9**, 1–12.
- D. Bolmatov, V. Brazhkin, Y. D. Fomin, V. Ryzhov and K. Trachenko, *J. Chem. Phys.*, 2013, **139**, 234501.
- T. J. Yoon, M. Y. Ha, E. A. Lazar, W. B. Lee and Y.-W. Lee, *J. Phys. Chem. Lett.*, 2018, **9**, 6524–6528.
- T. J. Yoon, M. Y. Ha, W. B. Lee and Y.-W. Lee, *J. Phys. Chem. Lett.*, 2018, **9**, 4550–4554.
- V. Brazhkin, Y. D. Fomin, V. Ryzhov, E. Tsiok and K. Trachenko, *Physica A*, 2018, **509**, 690–702.
- I. H. Bell, G. Galliero, S. Delage-Santacreu and L. Costigliola, *J. Chem. Phys.*, 2020, **152**, 191102.
- L. Bøhling, T. S. Ingebrigtsen, A. Grzybowski, M. Paluch, J. C. Dyre and T. B. Schrøder, *New J. Phys.*, 2012, **14**, 113035.

- 36 J. C. Dyre, *Phys. Rev. E*, 2013, **88**, 042139.
- 37 J. C. Dyre, *J. Phys. Condens. Matter*, 2016, **28**, 323001.
- 38 S. Prasad and C. Chakravarty, *J. Chem. Phys.*, 2014, **140**, 164501.
- 39 T. J. Yoon, M. Y. Ha, E. A. Lazar, W. B. Lee and Y.-W. Lee, *Phys. Rev. E*, 2019, **100**, 012118.
- 40 V. Brazhkin, A. Lyapin, V. Ryzhov, K. Trachenko, Y. D. Fomin and E. Tsiok, *Russ. J. Phys. Chem. BP*, 2014, **8**, 1087–1094.
- 41 R. Ryltsev and N. Chtchelkatchev, *J. Chem. Phys.*, 2014, **141**, 124509.
- 42 S.-T. Lin, M. Blanco and W. A. Goddard III, *J. Chem. Phys.*, 2003, **119**, 11792–11805.
- 43 J. Aragones, M. Conde, E. Noya and C. Vega, *Phys. Chem. Chem. Phys.*, 2009, **11**, 543–555.
- 44 J. Aragones and C. Vega, *J. Chem. Phys.*, 2009, **130**, 244504.
- 45 Y. Takii, K. Koga and H. Tanaka, *J. Chem. Phys.*, 2008, **128**, 204501.
- 46 S.-T. Lin, P. K. Maiti and W. A. Goddard III, *J. Phys. Chem. B*, 2010, **114**, 8191–8198.
- 47 S. Plimpton, *J. Comput. Phys.*, 1995, **117**, 1–19.
- 48 J. L. Abascal and C. Vega, *J. Chem. Phys.*, 2005, **123**, 234505.
- 49 C. Vega and J. L. Abascal, *Phys. Chem. Chem. Phys.*, 2011, **13**, 19663–19668.
- 50 D. Heyes, *CMST*, 2015, **21**, 169–179.
- 51 Y. Wu, H. L. Tepper and G. A. Voth, *J. Chem. Phys.*, 2006, **124**, 024503.
- 52 T. A. Pascal, D. Schärf, Y. Jung and T. D. Kühne, *J. Chem. Phys.*, 2012, **137**, 244507.
- 53 J. E. Funk, *Int. J. Hydrog. Energ.*, 2001, **26**, 185–190.
- 54 C. GRIMES, O. VARGHESE and S. RANJAN, *Light, water, hydrogen: the solar generation of hydrogen by water photoelectrolysis*, Springer Science & Business Media, 2007.
- 55 N. F. Carnahan and K. E. Starling, *J. Chem. Phys.*, 1970, **53**, 600–603.
- 56 T. Sun, J. Xian, H. Zhang, Z. Zhang and Y. Zhang, *J. Chem. Phys.*, 2017, **147**, 194505.
- 57 P.-L. Chau and A. Hardwick, *Mol. Phys.*, 1998, **93**, 511–518.
- 58 J. R. Errington and P. G. Debenedetti, *Nature*, 2001, **409**, 318–321.
- 59 R. Kumar, J. Schmidt and J. Skinner, *J. Chem. Phys.*, 2007, **126**, 05B611.
- 60 K. Himoto, M. Matsumoto and H. Tanaka, *Phys. Chem. Chem. Phys.*, 2011, **13**, 19876–19881.
- 61 Z. Pan, J. Chen, G. Lü, Y.-Z. Geng, H. Zhang and Q. Ji, *J. Chem. Phys.*, 2012, **136**, 164313.
- 62 E. A. Lazar, J. Han and D. J. Srolovitz, *Proc. Natl. Acad. Sci. U. S. A.*, 2015, **112**, E5769–E5776.
- 63 T. J. Yoon, M. Y. Ha, W. B. Lee, Y.-W. Lee and E. A. Lazar, *Phys. Rev. E*, 2019, **99**, 052603.
- 64 L. Weinberg, *SIAM J. Appl. Math.*, 1966, **14**, 729–738.
- 65 V. Schlegel, *Theorie der homogen zusammengesetzten Raumgebilde*, Engelmann, 1883.
- 66 T. L. Hill, *An introduction to statistical thermodynamics*, Courier Corporation, 1986.
- 67 C. Vega, J. Abascal and I. Nezbeda, *J. Chem. Phys.*, 2006, **125**, 034503.
- 68 R. Khusnutdinoff, *Colloid J.*, 2017, **79**, 152–159.
- 69 M. Janna and S. Bandyopadhyay, *Chem. Phys. Lett.*, 2011, **509**, 181–185.
- 70 M. Heyden, J. Sun, S. Funkner, G. Mathias, H. Forbert, M. Havenith and D. Marx, *Proc. Natl. Acad. Sci. U. S. A.*, 2010, **107**, 12068–12073.
- 71 E. Schwegler, G. Galli and F. Gygi, *Phys. Rev. Lett.*, 2000, **84**, 2429.